Investigations of a Dehumidifier in a Solar-Assisted Liquid Desiccant Demonstration Plant

Mustafa Jaradat
Institute of Thermal Engineering,
University of Kassel,
Kassel 34125, Germany

Daniel Fleig
Institute of Thermal Engineering,
University of Kassel,
Kassel 34125, Germany

Klaus Vajen
Institute of Thermal Engineering,
University of Kassel,
Kassel 34125, Germany

Ulrike Jordan[1]
Institute of Thermal Engineering,
University of Kassel,
Kassel 34125, Germany
e-mail: solar@uni-kassel.de

A solar-assisted liquid desiccant demonstration plant was built and experimentally evaluated. Humidity of the air, density of the desiccant, and all relevant mass flow rates and temperatures were measured at each inlet and outlet position. Adiabatic dehumidification experiments were performed in different seasons of the year under various ambient air conditions. The moisture removal rate $\dot{m}_v$, the mass balance factor κ_m, and the absorber effectiveness, ε_{abs}, were evaluated. An aqueous solution of LiCl was used as liquid desiccant with an initial mass fraction of about 0.4 kg_{LiCl}/kg_{sol}. The mass flow rate of the air through the absorber was about 1100 kg/h. The experimental results showed a reduction in the air humidity ratio in the range of 1.3–4.3 g/kg accompanied with an increase in the air temperature in the range of 3–8.5 K, depending on the inlet and operating conditions. For the air to desiccant mass flow ratio of 82, a mass fraction spread of 5.7% points in the desiccant and a volumetric energy storage capacity of 430 MJ/m^3 were achieved. By operating the desiccant pump in an intermittent mode, a mass fraction spread of about 13% points in the desiccant and an energy storage capacity of about 900 MJ/m^3 were reached. In addition, the experimental results were compared with results from a numerical model. The numerical model overestimates the heat and mass transfer because it assumes ideal surface wetting and uniform distribution of the circulated fluids.
[DOI: 10.1115/1.4040841]

Keywords: liquid desiccant, drying, plate-type absorber, energy storage capacity, finite-difference model

1 Introduction

The integration of desiccants into drying systems achieves many benefits, for example, it enables continuous drying even during off-sunshine hours and increases drying rates due to the reduced air humidity ratio and higher temperatures. Desiccant systems for product drying have been described already, for example, in Refs. [1–3]. Also, the integration of desiccant systems enhances the dried-product quality particularly for heat-sensitive products, as pointed out by Badgujar [4] and Misha et al. [5]. Furthermore, gentle drying at low temperature conditions is discussed in several studies and it was concluded that color change in agricultural products due to nonenzymatic browning reaction and taste quality are temperature dependent, for example, in Ref. [6].

Liquid desiccant systems allow more design and installation arrangements compared to solid desiccant wheels in which dehumidification and regeneration takes place simultaneously in the same heat and mass exchanger. In contrary, in liquid desiccant systems, the absorption and regeneration processes can be carried out independent of each other [7]. Concentrated liquid desiccants can be used as energy storage for peak load shifting [8]. Compared to sensible heat storage, thermochemical sorption energy storage can achieve very low energy losses during long-term storage. However, it must be noted that liquid desiccant systems are usually much more complex and expensive in comparison to sensible heat storage.

Conventional, high flow liquid desiccant systems such as packing towers (both structured and random types) have been the most studied types of liquid desiccant heat and mass exchangers in the past (e.g., Refs. [9–14]). In the packed beds, liquid desiccant flow rates are high to provide good surface wetting of the packing materials [15]. Heat released during the absorption process is removed with high flow rates. This enables low operating temperatures compared to adiabatic low-flow absorption processes. However, benefits of low compared to high flow systems are that a higher mass fraction spread of the desiccant solution, and therefore, a higher storage capacity are obtained per fluid cycle. Moreover, the risk of carry-over of the liquid desiccant droplets into the air stream can be reduced for low flow rates, a flat plate design, and fabric-flow channels. The benefits of low flow liquid desiccant systems were discussed by Lowenstein et al. [16,17]. Further investigations of low flow systems for increasing energy storage capacity were performed by the Bavarian Center for Applied Energy Research (ZAE Bayern) [8,18–20]. Field test investigations of a low flow liquid desiccant system for air conditioning applications with ambient air conditions were previously studied by several authors, such as Refs. [12] and [21].

Prior to the present research, various absorber designs and the wicking performance of different fabrics were evaluated experimentally [22]. Textiles with different compositions, thicknesses, and surface densities were tested at various desiccant solution mass fractions. The absorption capacity and diffusion behavior were evaluated. Moreover, a liquid desiccant distribution device was designed to facilitate a uniform distribution of the liquid desiccant at low flow rates, as possible, over the exposed surface. Various distribution pipe designs were investigated, as well.

In the presented research, a novel plate heat and mass exchanger was designed, built, and experimentally examined in combination with an aqueous solution of lithium chloride (LiCl) as a desiccant. The main aims of the design were

- to obtain a low humidity ratio of the process air,
- a high mass fraction (or concentration) spread of the liquid desiccant (high storage capacity), and
- to prevent carry-over of liquid desiccant droplets into the supply air.

[1]Corresponding author.

Contributed by the Solar Energy Division of ASME for publication in the Journal of Solar Energy Engineering: Including Wind Energy and Building Energy Conservation. Manuscript received June 28, 2017; final manuscript received May 27, 2018; published online October 1, 2018. Assoc. Editor: M. Keith Sharp.

To obtain an effective heat and mass transfer, a uniform distribution of the liquid desiccant over the exchanger surface is decisive. Therefore, the absorber is constructed of vertical plates with fabrics attached to enhance wetting of the surface. The desiccant is distributed to the fabrics with a very small flow rate. The air streams in cross-flow to the liquid desiccant.

The novel system and the experimental setup of the field test plant are described. Although working in a field test rig, high standard instrumentation was supplied, namely for the measurements of air flow rates (vortex sensors), solution flow rate (magnetic inductive flow meters), density sensors to evaluate sorbent mass fractions, and humidity sensors for air. Section 3 defines the key performance values evaluated in the presented study and basic equations of a numerical model used to compare calculated values with ideal assumptions with the measured data. The key performance values are, among others, absorber effectiveness as well as the energy storage capacity. In Sec. 4, experimental results of the dehumidification process are shown for a variety of reference conditions which are mainly influenced by the outdoor conditions in different seasons of the year, followed by a discussion in Sec. 5 of this paper.

2 Experimental Setup

2.1 Description of the Investigated System. Figure 1 shows a schematic diagram of the solar driven liquid desiccant system for drying hay bales in the demonstration plant.

In the absorber (1), the concentrated solution absorbs water from the ambient air and the diluted solution leaving the absorber is collected in the diluted-solution storage tank (2). During the dehumidification process, both the air and the solution temperature increase due to the released latent heat of vaporization and heat of dilution. The dried and heated air passes through an air–water postheater (3) and the dryer unit (4) which is loaded with a hay bale. The diluted solution is reconcentrated in the regenerator (5), where it is heated to increase its water vapor pressure. The heating water for the regeneration process is supplied from solar flat-plate collectors (6) with an aperture area of 127 m^2. Also, the diluted solution can be heated in an internal copper coil heat exchanger with an anticorrosion coating (length: 30 m and surface area: 1.3 m^2). The concentrated solution is cooled down by a similar heat exchanger placed in the solution tank (surface area: 2.1 m^2). The latter is connected to a dry cooling tower.

In the regenerator, an ambient air stream passes along the heated solution. There, water is desorbed from the desiccant solution into the air, and the solution is regenerated and delivered to the concentrated-solution storage tank (7). The specifications of the equipment in the investigated demonstration plant are listed in Table 1.

The components are installed in a 20 foot container at the Hessian State Domain Frankenhausen, Germany. A plate-type heat and mass exchanger is used as an absorber (adiabatic mode). The hot water for the air postheater is supplied from the solar thermal flat plate collectors in order to rise the air temperature leaving the absorber to a supply temperature in the range of 37–42 °C.

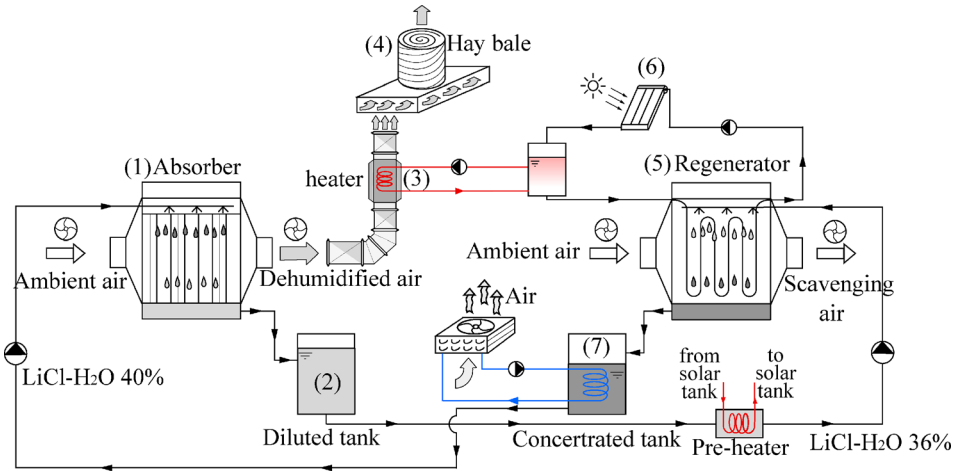

Fig. 1 Schematic diagram of the solar-driven liquid desiccant demonstration plant

Table 1 Specifications of the absorber and regenerator

Parameter	Absorber	Regenerator[a]
Type	Plate type	Tube-bundle
Material	Polycarbonate	Coated copper
Operation	adiabatic	Internally heated
Number of plates/tubes	60 plates	39 tubes
Height × width of plates (mm)	600 × 600	—
Diameter of tubes, uncoated (mm)	—	12 mm
Diameter of tubes, coated (mm)		12.6
Thickness of wicking material (mm)	0.4	0.4
Height × width × length (cm)	100 × 60 × 70	85 × 30 × 75
Effective surface area (m^2)	72	7.5
Volume (m^3)	0.42	0.19
LiCl-H_2O inlet mass fraction (kg/kg)	0.40	0.36
Re number for LiCl-H_2O solution	1.04×10^{-5}–3.87×10^{-5}	3.02×10^{-5}–6.22×10^{-5}
Nu number for LiCl-H_2O solution	5.10×10^{3}	4.83×10^{3}

[a]The regenerator in the demonstration plant is not discussed in this paper as a result of an air leakage in the air-air heat recovery unit.

Fig. 2 View of the liquid desiccant demonstration plant: (1) plate-type absorber, (2) diluted LiCl-H_2O solution tank, (3) process air postheater, (4) hay bale connected to the dryer unit, (5) tube-bundle regenerator, and (6) solar thermal flat plate collectors

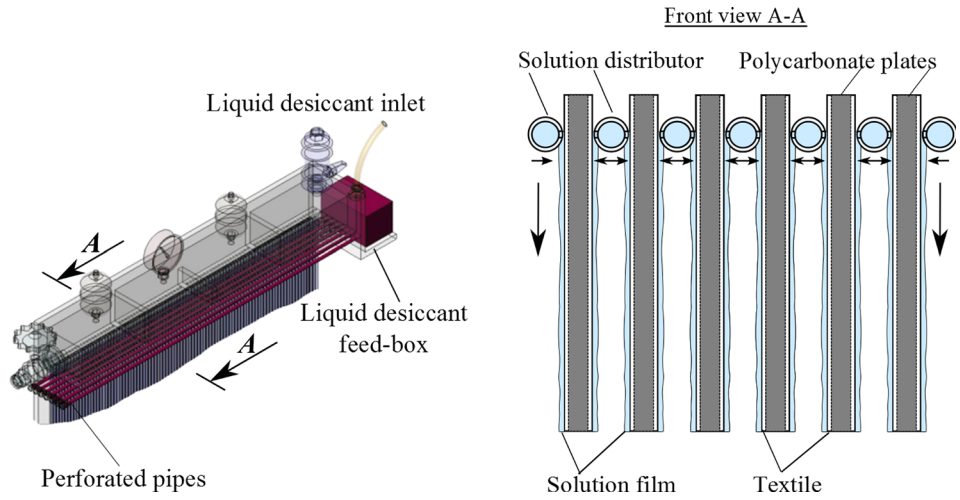

Fig. 3 Skeleton view of the plate absorber (left) and a front view of the absorber showing a part of the desiccant distribution pipes which are located between the vertical plates (right)

The investigations presented in this paper are focused on the absorption process. Figure 2 shows part of the components of the liquid desiccant system installed in the container (left), the hay drying unit placed in front of the container (middle), and the solar thermal flat plate collectors installed on the roof of the premises (right).

A novel absorber (conditioner) was designed for this field test rig. The absorber was made of 60 polycarbonate plates with dimensions of 840 mm × 700 mm (height × length). Textile sheets are attached on each side of the plates. The textiles were selected based on laboratory tests regarding their absorption capacity and diffusion behavior of LiCl-H_2O solution. Spacers are mounted between the plates, so that the air flows through channels with a width of 5.2 mm. Aqueous LiCl solution is introduced from above and it flows through a distributor. The latter consists of 62 polymethyl methacrylate pipes with 23 perforations on both sides. The sizes of the discharge bores as well as the distance between the adjacent bores were experimentally optimized by Jaradat et al. Figure 3 shows the plate-type absorber and the liquid desiccant distributor.

The solar-assisted liquid desiccant dryer in the present research is used for drying agricultural products such as hay bales. The conditioner (absorber) reduces the air humidity ratio and heats up the air by a few Kelvins above the ambient temperature. A moisture content of about 18–12% wet basis (w. b.) within the hay bales represents the maximum recommended content for safe storage. Investigations on flow patterns and the drying behavior of the hay bales were presented in Ref. [23]. In earlier experiments, the time to reduce the moisture content of the hay bales from about 30–35% w. b. to about 13% w. b. was reduced to about 4 h, compared to about 20 h by using conventional heated air system.

2.2 Instrumentation and Experimental Set-Up. Ambient air passes a filter and it is then supplied to the absorber. The air humidity ratio is derived from the measured air dry-bulb temperature and relative humidity by applying humid air equations given by ASHRAE Handbook of Fundamentals [24].

The liquid desiccant hydraulic circuit consists of tanks for the concentrated and diluted desiccant solutions with a volume of 600l, each. Filters, made of polyamide, with a pore size of 300 μm are installed in the tanks to get rid of possible contaminates that could clog the discharge-bores of the liquid desiccant distributor. The desiccant solution is pumped to the absorber with a membrane pump. The desiccant mass fraction is derived by the measured desiccant density and temperature by applying the correlations given by Conde [25]. The positions of the instruments used in the demonstration plant are shown in Fig. 4.

The raw data from all of measurement devices are sampled by a multiplexer and logged with LabVIEW® with a time-step of 10 s. Here, mainly the averaged values of the sample time of about 30 min are shown. The types, rated accuracy, and operation range of the used measurement devices are given in Table 2.

Although the plant was equipped with high-grade instrumentation, the overall uncertainty of evaluated system efficiency deviated from laboratory values. The uncertainty analysis in this paper is performed regarding the highest error source: The sensors precision is given by the manufacturer or the standard deviation within the logged data. The temperature and flow rate sensors were calibrated additionally in the laboratory before the installation in the demonstration plant. The remaining uncertainties for the measured data, including uncertainties of the data acquisition system, turned out to be above the uncertainties given by the manufacturers. Moreover, the uncertainty given by the manufacturer regarding the air relative humidity was checked with a higher

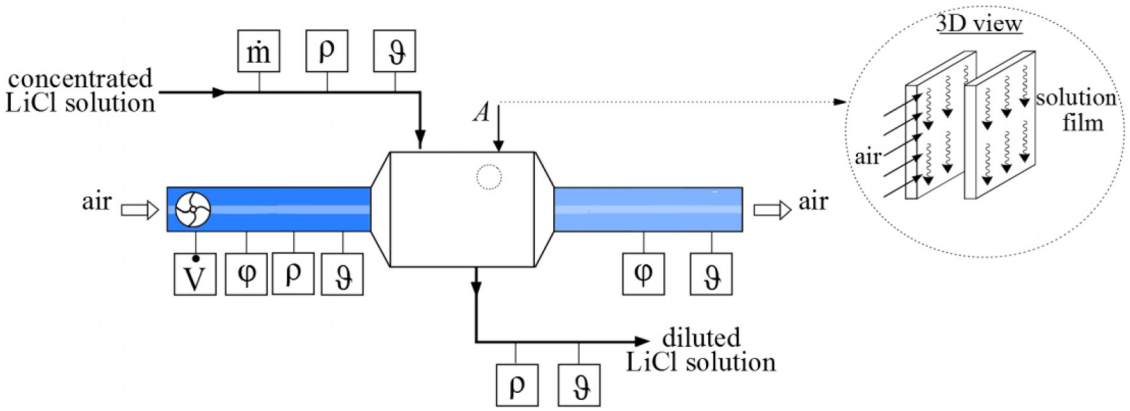

Fig. 4 Schematic diagram of the instrumentation setup of the circulated fluids

Table 2 Summary of the measurement devices and their uncertainties

Parameters	Model	Uncertainty	Range of operation
Air flow rate	Optiswirl 4070 DN 150	2% of the measured value	370–4800 m^3/h
Air temperature	HygroFlex 420	±0.2 K	−50–100 °C
Air relative humidity	HygroFlex 420	1% of the measured value	0–100%
Solution flow rate	Optiflux 1050	0.5% of the measured value	20–3900 l/h
Solution temperature	Pt100	±0.3 K	
Solution density	L-Dens 323	0.001 g/cm^3	0.5–2 g/cm^3

precision sensor. Further tests were carried out within a few months before the measurements on site. In these tests, the maximum error limit given by the manufacturers was confirmed. Large potential error sources are two of the hygrometers that were installed several years ago. However, drifts due to the conditions of use or due to sensor aging were not detected. Possible further errors, e.g., induced by aging were not taken into account in the error analysis.

2.3 Inlet and Operating Conditions. Experiments were performed in different seasons of the year with different ambient air temperatures and humidity ratios. The experiments took place in fall 2013, in winter 2015, and in summer 2015. In the performed experiments, the air to solution mass flow ratio was varied between $r_m = 9.2$ and 87.5, with $r_m = \dot{m}_a/\dot{m}_{sol}$, for a constant air mass flow rate of about 1100 kg/h. The mass fraction of the LiCl-H_2O solution delivered to the absorber was in the range of $\xi = 0.4\ kg_{LiCl}/kg_{sol}$, corresponding to a concentration of about 0.5 kg/l.

With the first experiments performed in fall 2013, the transient behavior of the absorption process was analyzed and a concept of intermittent pumping operation was tested.

As shown in Table 3, the values for the ambient air temperature $\vartheta_{a,i}$ and the humidity ratio $\omega_{a,i}$ were much lower for winter ($\vartheta_{a,i} = 5\,°C$–$12\,°C$; $\omega_{a,i} = 3.7$ g/kg–5.2 g/kg) than for summer operation ($\vartheta_{a,i} = 19\,°C$–$26\,°C$; $\omega_{a,i} = 11.6$ g/kg–12.6 g/kg).

3 Evaluation and Numerical Model

The change of the supply air temperature $\Delta\vartheta_a$, the change of the supply air humidity ratio $\Delta\omega_a$, the moisture removal rate $\dot{m}_v$, the mass balance factor κ_m, the absorber effectiveness ε_{abs}, and the energy storage capacity C_S were evaluated to analyze the experiments.

The moisture removal rate from the supply air stream to the concentrated LiCl-H_2O solution in the absorption process, $\dot{m}_v$, is calculated from the air side (AS) and from the solution side (SS). On the air side, it is a function of the air humidity ratio spread, $\Delta\omega = \omega_i - \omega_o$, in the following equation:

$$\dot{m}_{v,AS} = \dot{m}_{da}(\omega_i - \omega_o) \tag{1}$$

On the solution side, it is a function of the water content spread of the desiccant $\Delta X = X_o - X_i$ in the following equation:

$$\dot{m}_{v,SS} = \dot{m}_{LiCl}(X_o - X_i) \tag{2}$$

where X is the mass of water per the mass of LiCl (in kg_{H2O}/kg_{LiCl}). It is given in the following equation:

$$X = \frac{1-\xi}{\xi} \tag{3}$$

where ξ (in kg_{LiCl}/kg_{sol}) is the mass fraction of LiCl in the solution. The mass fraction spread of the desiccant solution in the absorber $\Delta\xi$ is the difference between the inlet and outlet values.

The mass balance factor κ_m is defined as the ratio between the moisture removal rates on air side and solution side as defined by Eq. (4):

$$\kappa_m = \frac{\dot{m}_{da}\Delta\omega}{\dot{m}_{LiCl}\Delta X} \tag{4}$$

Table 3 Summary of the inlet operating conditions of the performed experiments in the demonstration plant

	Range of ambient air inlet conditions			Range of LiCl-H_2O inlet conditions			Mass ratio (G/L)
Period	$\dot{m}_a$ (kg/h)	ϑ_a (°C)	$\omega_a(g/kg)$	$\dot{m}_{sol}$ (kg/h)	ϑ_{sol} (°C)	ξ_{sol} (kg/kg)	r_m
Fall 2013	1100	8–17	6–9	12–120	11–16	0.39–0.42	9–87
Winter 2015	1100	5–12	4–5	22–118	9–12	0.41	10–50
Summer 2015	1100	19–26	11–13	13–116	22–24	0.40	9–82

The absorber effectiveness, ε_{abs}, is defined by the below equation:

$$\varepsilon_{abs} = \frac{\omega_{a,i} - \omega_{a,o}}{\omega_{a,i} - \omega_e} \tag{5}$$

where ω_e is the saturation humidity ratio of air at equilibrium with the desiccant solution at the desiccant solution inlet temperature in the following equation:

$$\omega_e = 0.62198 \frac{p_s(\vartheta_{sol,i}, \xi_{sol,i})}{p - p_s(\vartheta_{sol,i}, \xi_{sol,i})} \tag{6}$$

where p_s is the saturated pressure as a function of the solution inlet temperature and concentration, obtained from Conde [25] for aqueous solutions of LiCl.

The energy storage capacity C_S is defined as the dehumidification enthalpy over the volume of the diluted solution (at the absorber outlet) and is given by the below equation [20]:

$$C_s = \frac{\text{dehumidification enthalpy}}{\text{volume of the diluted solution}} = \frac{m_v h_{fg}}{V_{dil.sol}} = h_{fg} \Delta X \xi_{dil,sol}\ \rho_{dil,sol} \tag{7}$$

The experimental results were compared with numerical results from a finite-difference model. The model was developed at the University of Kassel by Mützel [26] based on the work of Mesquita [27]. The model describes the heat and mass transfer of the plate-type absorber. The number of nodes can be varied; however, in the present study, it was set to 200 nodes in the air flow direction (X-axis) and 200 nodes in the solution flow direction (Y-axis). For the interfacial layer, the number of nodes was set to 60 nodes; 30 nodes for air (XZ), 29 nodes for the desiccant solution (YZ), and one node for the phase boundary, Fig. 5.

The model is based on the following assumptions:

- fully developed laminar flow for the desiccant and air streams;
- complete wetting of the surface area by the desiccant;
- a constant film thickness which is equal to textile thickness;
- convection perpendicular to the phase boundary (PB) is neglected;
- conduction and diffusion in flow direction is neglected;
- uniform diffusion coefficients $D_{\vartheta,\xi}$ and conductivities $\lambda_{\vartheta,\xi}$ for same x- and y-coordinate for the air and desiccant solution, respectively;
- constant node distances in each phase.

The heat flow in the z-direction perpendicular to the phase boundary described by Fourier's law yields

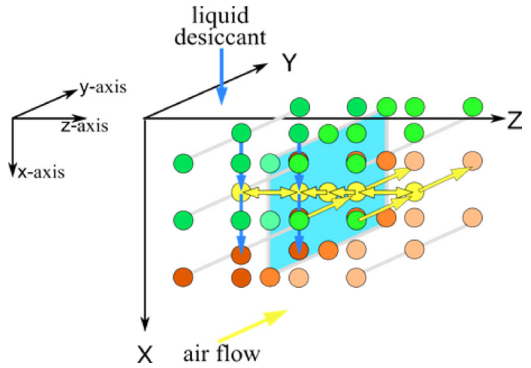

Fig. 5 Schematic of the model simulation nodes, adapted from Ref. [26]

$$\dot{Q}_z = A\lambda_{\vartheta,\xi} \frac{d\vartheta}{dz} \approx A\lambda_{\vartheta,\xi} \frac{\Delta\vartheta}{\Delta z} \tag{8}$$

With the given assumptions, the heat balance is described by the following equations:

$$\dot{Q}_{conv,in} + \dot{Q}_{cond,in} = \dot{Q}_{conv,out} + \dot{Q}_{cond,out} \tag{9}$$

$$\vartheta_{in}\dot{C}_{in} + \frac{A\lambda}{\Delta z}(\vartheta_{z+1} - \vartheta_z) = \vartheta_z \dot{C}_{out} + \frac{A\lambda}{\Delta z}(\vartheta_z - \vartheta_{z-1}) \tag{10}$$

The corresponding mass flow of the water vapor based on Fick's law yields

$$\dot{m}_{v,z} = M\dot{n} = -\text{MAD}_{\vartheta,\xi} \frac{d\xi}{dZ} \approx -\text{MAD}_{\vartheta,\xi} \frac{\Delta\xi}{\Delta Z} \tag{11}$$

The mass balance yields the following equation:

$$C_{w,X-1}\dot{m}_{sol,in} + \rho \frac{AD}{\Delta Z}(C_{w,Z+1} - C_w) = C_w \dot{m}_{sol,out} + \rho \frac{AD}{\Delta Z}(C_w - C_{w,z-1}) \tag{12}$$

Flow velocities of the liquid desiccant are calculated assuming a plug-flow with a constant film thickness of 0.4 mm.

At the PB, the local equilibrium conditions $p_{v,sol}(\text{PB}) = p_{v,air}(\text{PB})$ and $T_{sol}(\text{PB}) = T_{air}(\text{PB})$ yield the following coupled equations for the heat and mass balances, solved with a Newtonian algorithm:

$$\Delta\dot{q} = \dot{h}_{sor} - \dot{q}_{PB\to sol} - \dot{q}_{PB\to air} = 0 \tag{13}$$

$$\Delta\dot{q} = \frac{\dot{m}_{v,air}}{A_{xy}} \Delta h_{sol} - \frac{\lambda_{air}}{\Delta z_{air}}(\vartheta_{PB} - \vartheta_{z+1}) - \frac{\lambda_{sol}}{\Delta z_{sol}}(\vartheta_{PB} - \vartheta_{z-1}) \tag{14}$$

$$\Delta\frac{\dot{m}_v}{A_{xy}} = \frac{\dot{m}_{v,air}}{A_{xy}} - \frac{\dot{m}_{v,sol}}{A_{xy}} = 0 \tag{15}$$

$$\Delta\frac{\dot{m}_v}{A_{xy}} = \frac{D_{air}}{\Delta z_{air}} \cdot \left(\rho_{air} C_{w,z+1} - \frac{p_{v,PB} M_w}{R T_{PB}}\right) - \frac{D_{sol}\rho_i}{\Delta z_{sol}}((1 - \xi_{PB}) - (1 - \xi_{z-1})) \tag{16}$$

With the subscripts v for water vapor, w for liquid water, PB for phase boundary, and sol for solution.

4 Experimental Results

In the following, the results of 20 dehumidification measurements are presented. Each of the experimental results shown in Tables 4 and 5 is derived from nearly stationary conditions after a start-up time of about 30–60 min.

4.1 Example Experimental Run. Figure 6 shows an example of the measured inlet and outlet values of the temperatures and relative humidity for a measurement in fall 2013. Figure 7 shows the temporal course of the values to reach nearly stationary conditions during the experimental run. The air to solution mass flow ratio and the desiccant inlet mass fraction were $r_m = 9.2$ and $\xi_i = 0.385\ kg_{LiCl}/kg_{sol}$, respectively.

The values show a reduction in the air relative humidity by about 40% points and an increase in the air inlet temperature of about 5 K. The air leaving the absorber is further heated to 36 °C by an air–water heat exchanger. There, the air relative humidity further decreases. In the given example, the air humidity ratio is

Table 4 Winter conditions: Experimental results for the plate absorber in the field test demonstration plant between February and March 2015

Date 2015	Run	$\Delta\vartheta_a$K	$\Delta\omega$ (g/kg)	$\Delta\xi$ (kg/kg)	$\dot{m}_{v,\mathrm{AS}}$(kg/h)	$\dot{m}_{v,\mathrm{SS}}$(kg/h)	$\dot{m}_{v,\mathrm{sim}}$ (kg/h)	M (%)	κ_m	ε	C_s (MJ/m^3)	r_m
25.02	I	5.6	1.3	0.0057	1.41	1.66	2.80	45.1	0.85	0.54	43.5	10
	II	5.1	1.4	0.0103	1.57	1.52	2.51	38.4	1.03	0.65	79.1	19
	III	5.7	1.5	0.0174	1.72	1.59	2.70	38.9	1.08	0.64	132.3	31
	IV	5.2	1.4	0.0180	1.57	1.27	2.53	43.7	1.23	0.64	136.7	41
	V	5.5	1.4	0.0253	1.61	1.47	2.63	41.3	1.09	0.66	192.2	51
19.03	VI	3.4	2.1	0.0147	2.38	2.17	3.39	32.8	1.10	0.51	111.8	19
	VII	3.7	1.9	0.0208	2.15	2.05	3.17	33.7	1.05	0.47	157.8	29
	VIII	4.6	1.9	0.0311	2.14	2.32	3.15	29.3	0.92	0.48	235.5	40
30.03	IX	3.0	1.7	0.0064	1.90	1.82	3.03	38.6	1.04	0.52	49.3	10
	X	3.8	1.9	0.0144	2.13	2.09	3.28	35.6	1.02	0.51	110.0	20
	XI	4.4	1.9	0.0234	2.13	2.28	3.32	33.6	0.93	0.50	178.1	30
	XII	3.4	1.7	0.0343	1.87	2.16	3.10	35.1	0.86	0.46	258.9	47

Table 5 Summer conditions: Experimental results for the plate absorber in the field test demonstration plant: Experiments I–IV were conducted on Aug. 11, 2015 and the experiments V–VIII were performed on Aug. 27, 2015

Date 2015	Run	$\Delta\vartheta_a$K	$\Delta\omega$ (g/kg)	$\Delta\xi$ (kg/kg)	$\dot{m}_{v,\mathrm{AS}}$(kg/h)	$\dot{m}_{v,\mathrm{SS}}$(kg/h)	$\dot{m}_{v,\mathrm{sim}}$ (kg/h)	M (%)	κ_m	ε	C_s (MJ/m^3)	r_m
11.08	I	6.8	4.3	0.0098	4.72	2.93	5.56	31.2	1.61	0.48	76.3	9
	II	7.1	3.8	0.0257	4.09	3.92	4.96	19.3	1.04	0.41	198.6	19
	III	6.7	3.3	0.0414	3.57	3.33	4.50	23.3	1.07	0.36	316.4	38
	IV	5.5	2.9	0.0475	3.13	3.05	4.22	26.8	1.03	0.31	361.9	48
27.08	V	8.5	4.1	0.0169	4.58	3.43	5.89	32.0	1.34	0.52	131.4	14
	VI	8.0	3.4	0.0301	3.81	3.19	5.44	35.7	1.19	0.44	232.4	28
	VII	6.2	2.9	0.0488	3.16	3.06	4.49	30.7	1.03	0.39	372.6	50
	VIII	5.9	2.7	0.0566	2.94	2.22	4.02	35.9	1.33	0.36	430.0	82

reduced by about $\Delta\omega$= 3.3 g/kg, corresponding to a moisture removal rate from the supply air of $\dot{m}_{v,\mathrm{AS}}$ =3.6 kg/h.

4.2 Winter Conditions. The results of the field experiments for the time period between February and March 2015 are shown in Table 4.

For the winter conditions, the humidity ratio is reduced by about $\Delta\omega$= 1.3–2.1 g/kg, while the air temperature in the absorber increases by about 3.0–5.7 K. The highest mass fraction spread of about $\Delta\xi$=3.4% points is recorded for the air to solution mass flow ratio of r_m= 47. The minimum mass fraction spread of the desiccant of $\Delta\xi < 0.01$ was reached for the air to desiccant mass ratio of r_m= 10. The energy storage capacity C_s decreased from 259 to 49.3 MJ/m^3 for the third measurement sequence (Mar. 30, 2015) by increasing the desiccant solution flow rate by factor of 4.7, while the remaining inlet conditions were fairly constant.

4.3 Comparison With Numerical Results. Figure 8 shows the measured moisture removal rates $\dot{m}_{v,\mathrm{AS}}$ and $\dot{m}_{v,\mathrm{SS}}$, given in Table 4, as well as the values calculated with the finite-difference model $\dot{m}_{v,\mathrm{sim}}$ for the experiments carried out on three days in winter 2015. The liquid desiccant mass flow rate was varied at each of the days between about $\dot{m}_{\mathrm{sol}}$=10 and 120 kg/h. Due to strongly varying inlet conditions of the air, the results are not plotted over one of the parameters. Instead, Fig. 8 shows solely the values of $\dot{m}_v$ over the experimental run.

The measured moisture removal rate is between $\dot{m}_v = 0.39$ and 0.63 g/s. The higher the desiccant solution flow rate $\dot{m}_{\mathrm{sol}}$, the higher is $\dot{m}_v$ for (nearly) constant air mass flow rates $\dot{m}_a$.

The optimization potential for the absorption process M (mean absolute deviation between the measured and numerical values), as defined in the following equation, are listed in Table 4:

$$M = \left| \frac{\dot{m}_{v,\mathrm{exp}} - \dot{m}_{v,\mathrm{sim}}}{\dot{m}_{v,\mathrm{sim}}} \right| \cdot 100\% \tag{17}$$

The values of M are in the range between 29 and 45%.

The mass balance factor κ_m, as defined in Eq. (4), was in the range between 0.85 and 1.23 for the winter experiments. This illustrates Fig. 9, which shows the moisture removal rate evaluated on the solution side, $\dot{m}_{v,\mathrm{SS}}$, over the value evaluated on the

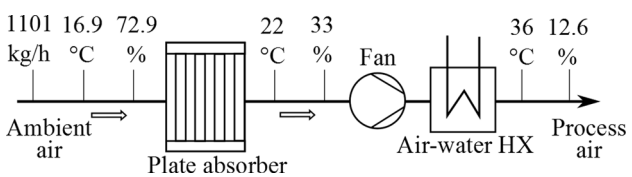

Fig. 6 Example of the measured inlet and outlet values for the absorption line in the demonstration plant

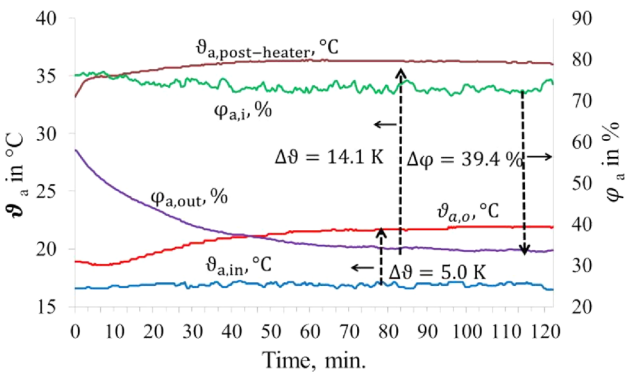

Fig. 7 Temporal course of the temperatures and humidity during a test sequence to reach nearly stationary conditions

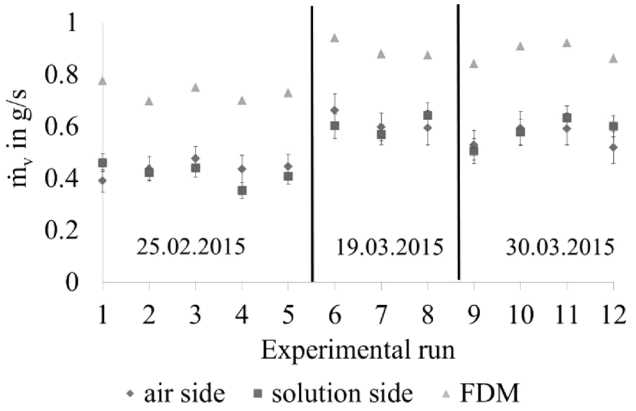

Fig. 8 Rate of moisture removal rate versus the experimental run for the experiments carried out on three days in winter 2015

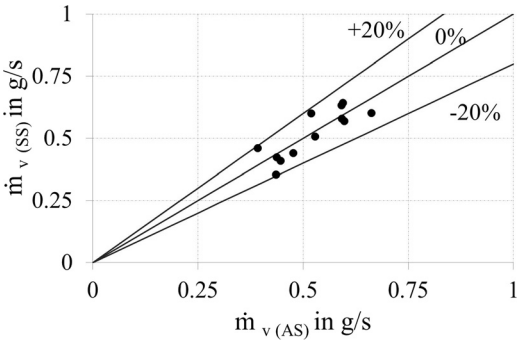

Fig. 9 Mass balance for the experiments implemented in the demonstration plant for the experiments performed in winter 2015

air side, $\dot{m}_{v,\mathrm{AS}}$. The discrepancies were within the experimental uncertainty (within ±20%) and in good symmetry.

4.4 Summer Conditions. The results of the field experiments for August 2015 are given in Table 5.

The humidity ratio is reduced by about $\Delta\omega = 2.9$ g/kg–4.3 g/kg, while the air temperature in the absorber increases by about 5.5–8.5 K. The increase in the air temperatures is clearly higher than those for the winter experiments as a result of higher air inlet humidity ratios and thus increased enthalpy of condensation and enthalpy of dilution.

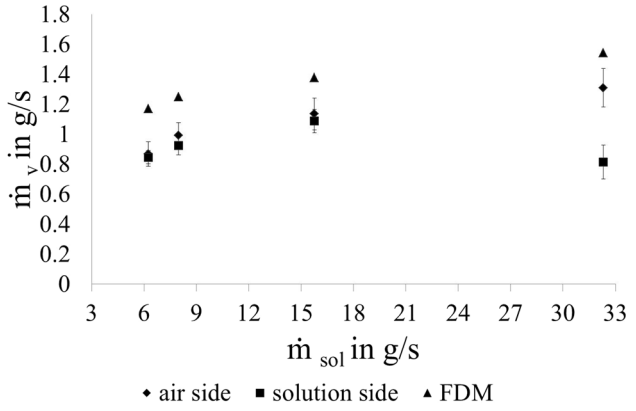

Fig. 10 Moisture removal rate calculated by applying Eq. (1) AS and by applying Eq. (2) SS for the experiments implemented in the demonstration plant on Aug. 11, 2015

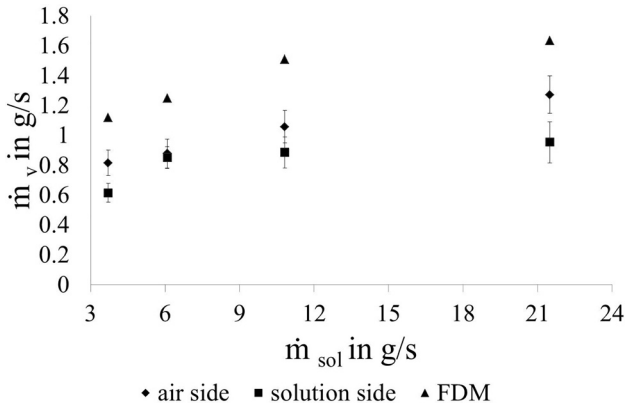

Fig. 11 Moisture removal rate calculated by applying Eq. (1) AS and by applying Eq. (2) SS for the experiments implemented in the demonstration plant on Aug. 27, 2015

Figures 10 and 11 show the moisture removal rate $\dot{m}_v$ over the solution mass flow rate $\dot{m}_{\mathrm{sol}}$ for two different days in August 2015. Air inlet temperatures, $\vartheta_{a,i}$, and inlet humidity ratios, $\omega_{a,i}$, vary only slightly in the course of these days. For this reason, trend curves can be shown for these experiments. $\dot{m}_v$ increases in general for higher desiccant flow rates (i.e., for smaller air to solution mass flow ratios r_m). Also, as shown in Table 5, the moisture removal rate calculated from the air side is higher than those estimated from the solution side $\dot{m}_{v,\mathrm{AS}} > \dot{m}_{v,\mathrm{SS}}$ for all of the experiment runs. The low value of $\dot{m}_{v,\mathrm{SS}}$ for the largest value of the desiccant flow rates in both diagrams is explained mainly by experimental uncertainties in the mass flow rate of the desiccant solution.

The absorber effectiveness increases by increasing the desiccant solution mass flow rate as shown in Figs. 12 and 13. Increasing the solution mass flow rate leads to lower values of the humidity ratio at the absorber outlet ω_o, and thus, increases the change in the humidity ratio $\Delta\omega$, presented in Eq. (5).

The optimization potential is in the range of $M = 19\%$–35%-points for summer operation. It is significantly lower than the one for winter operation ($M = 29\%$–45%).

The mass balance factor κ_m is in the range between 1.03 and 1.34 for summer conditions, with exception of the first experimental run (I in Table 5). In the latter, the flow of the desiccant solution was disrupted accidently during the measurement. Figure 14 shows the moisture removal rate evaluated on the solution side, $\dot{m}_{v,\mathrm{SS}}$, over the value evaluated on the air side, $\dot{m}_{v,\mathrm{AS}}$, for the summer experiments. Several values exceed the ± 20% margins. Moreover, all of the values are below the 0%-line which indicates a systematic error.

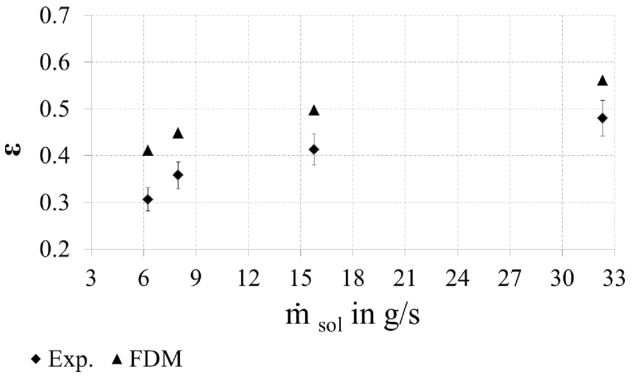

Fig. 12 Absorber effectiveness for the experiments implemented in the demonstration plant on Aug.11, 2015

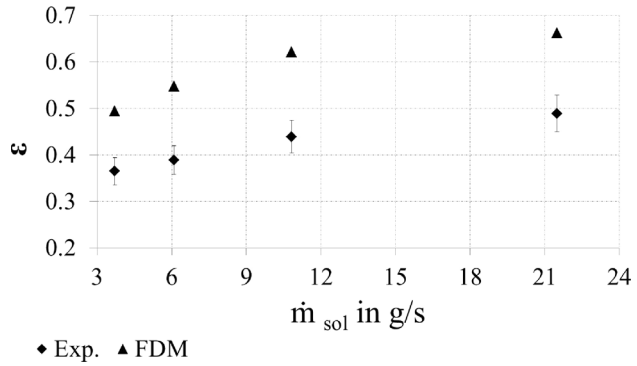

Fig. 13 Absorber effectiveness for the experiments implemented in the demonstration plant on Aug. 27, 2015

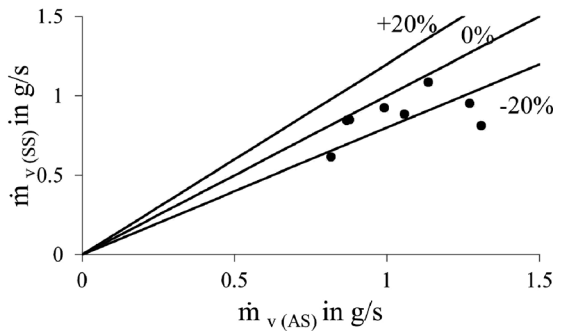

Fig. 14 Mass balance for the experiments implemented in the demonstration plant in summer 2015

Figures 15 and 16 show, respectively, the storage capacity C_s and the mass fraction spread $\Delta\xi$ for the summer measurements as a function of the desiccant mass flow rate. C_s is in the range between 76.3 and 430 MJ/m^3. The mass fraction spread, $\Delta\xi$, varies between 0.010 and 0.057 and is inversely proportional to the desiccant mass flow rate.

4.5 Intermittent Pumping of the Desiccant Solution. In the experiments presented in Fig. 17, the desiccant is pumped in 10 min intervals followed by a 20 min pause. The aim of this operation mode is to increase the energy storage capacity of the liquid desiccant system and to ensure sufficient wetting of the textile surfaces. At the same time, the air temperature and humidity ratio, provided to the product being dried, is not affected.

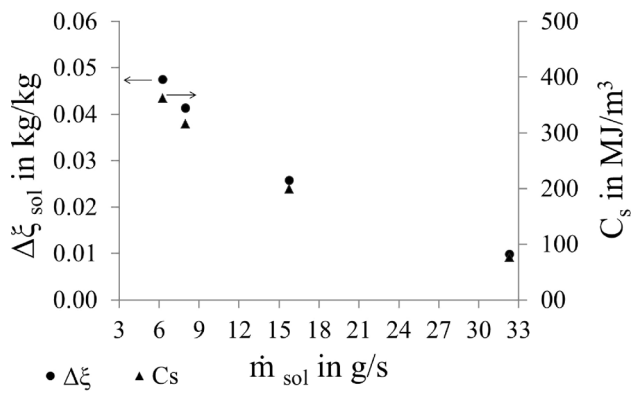

Fig. 15 Mass fraction spread and energy storage capacity for the experiments implemented in the demonstration plant on Aug. 11, 2015

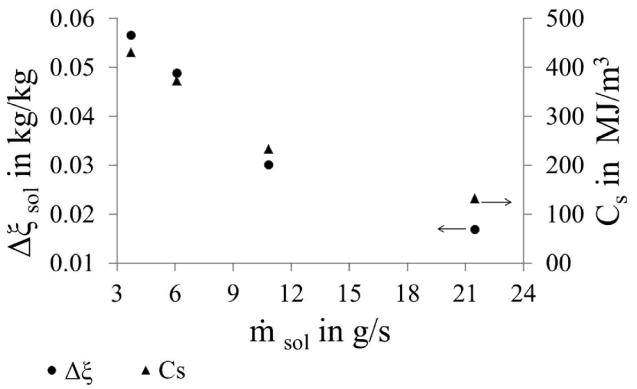

Fig. 16 Mass fraction spread and energy storage capacity for the experiments implemented in the demonstration plant on Aug. 27, 2015

Figure 17 shows the intermittent operation of the absorber for an experimental run with three time periods (on/off-intervals). After the initial start, the air outlet temperature fluctuates by only about 1 K. The outlet relative humidity is only slightly affected by the stand-by period. During operation, the desiccant mass flow rate was about 114kg/h. This leads to a mean flow rate for the entire period of about 38kg/h. In this measurement, the mass fraction spread was about $\Delta\xi$= 13%-points, the desiccant mass fraction at the absorber outlet was about $\xi_o = 0.286\,\mathrm{kg_{LiCl}/kg_{sol}}$, and the energy storage capacity was about $C_s = 900\,\mathrm{MJ/m^3}$.

If a plug-flow of the liquid desiccant is assumed with a film thickness equal to the thickness of the textile of 4×10^{-4}m, the cross-sectional area for the flow is about 3.4×10^{-3}m^2 (with 118 plate surfaces) and the flow velocity is only about 6×10^{-3}m/s. This means that the time of a flow from the top to the bottom of the absorber is about of 18 min.

This number corresponds quite well with the time delay that was determined between the start of the measurements and stationary conditions of 20–40 min.

5 Discussion

The experimental results are in general in line with the expected trends like the increase of the moisture removal rate $\dot{m}_v$ for an increase in the liquid desiccant flow rate in Figs. 10 and 11.

The larger the mass flow rate of the desiccant solution $\dot{m}_{sol}$, the smaller is the mass fraction spread of the desiccant $\Delta\xi$, while the solution temperature rises less. Due to higher mass fractions and lower temperatures of the liquid desiccant on the absorber

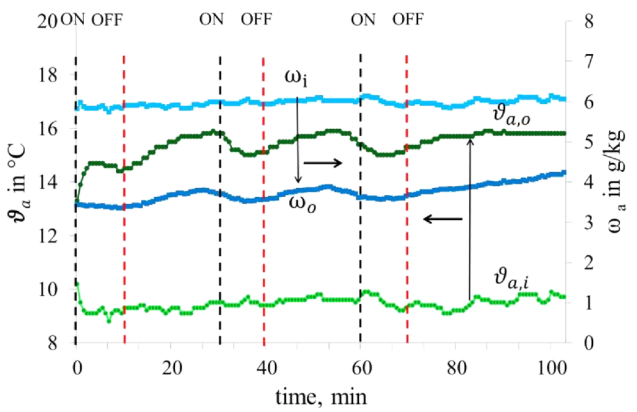

Fig. 17 Intermittent pump-operation of the absorber in the field test plant, fall 2013. The operating conditions of the given example were $\dot{m}_a$ = 1100 kg/h, $\vartheta_{a,i}$ = 9.5 °C, $\omega_{a,i}$ = 6 g/kg, $\dot{m}_{sol}$ = 114 kg/h, and ξ_i = 0.42 kg/kg.

plate at high desiccant mass flow rates, the water vapor pressure of the solution is reduced and the absorber effectiveness ε_{abs} is increased.

Only few related studies are available in the literature which present investigations of heat and mass exchangers in cross flow configuration in general, and even less for low flow systems. For the recently developed components presented in the present study, the effectiveness values $\bar{\varepsilon}_{abs}$ of up to 0.66 for winter conditions are significantly increased compared to high flow systems that are presented in the literature, for example, the system by Liu et al. [28] with an air-to-solution mass ratio range of $r_m = 0.8$–1.1. The mass ratios of the desiccant solution in the present paper are $r_m = 10$–80, which should have a negative impact on the absorber effectiveness. For a low flow system presented by Keßling et al. [8], with $r_m = 40$–150, for example, the absorber effectiveness was in the range of $\bar{\varepsilon}_{abs} = 0.33$, although the absorber was internally cooled in an isothermal process.

In the present study, the mean absolute deviation between the measured and numerical values, M (Eq. 17), are larger than the experimental uncertainty due to ideal model assumptions for example

- Equal flow distributions and wetting of the textiles attached to the plates. The model assumes a constant film thickness over the plate-length, equal to the textile thickness of 0.4 mm.
- Uniform air-flow through the absorber. The model assumes constant air face velocity along the whole length of the plate and for all of the plates.
- A pure LiCl-H_2O solution. The solution properties (vapor pressure, density, viscosity, thermal capacity, differential enthalpy of dilution, etc.) are based on higher purity grade compared to the values of the experiments [25]. In the present study, the LiCl salt used has an industrial purity grade of about 98.5% and was mixed with tap water.
- the effect of aging of the LiCl-H_2O solution under field operation conditions in the demonstration plant.

Nevertheless, in general, the tendencies of the evaluated parameters for different inlet conditions are similar in the experiment and model. In addition, the results corresponds with findings reported in the literature. For example, Mesquita [29] presented deviations of measured and calculated values of the moisture removal rate of up to 40%. He explained 70% of this deviation by uncertainties within the humidity measurements. Moreover, he reported that a formation of dry patches was observed after the fabric (cotton) dried out.

The authors assume that the main reason for the increased deviations between measured and simulated values for winter conditions is the lower air inlet humidity ratio during winter time, because it is connected with higher measurement uncertainties.

The systematic error shown by the mass balance factor κ_m for summer conditions could be a result of short experimental runtime for the experiments performed in the summer compared to those performed in winter. The density of the desiccant solution at the absorber outlet is measured only twice. The measured densities for the experiments that are performed in the summer were more likely in the transient state. The authors believe that this causes a systematic error in the low moisture removal rates.

The volumetric energy storage capacity C_s is a decisive measure to reach small storage sizes. This is important especially for long-term storage. C_s is high for small desiccant flow rates $\dot{m}_{sol}$. However, the experimentally evaluated values of C_s are lower than expected, presumably as a result of inadequate wetting of the plates. With an inlet air humidity ratio of $\omega_{a,i} = 14.5$ g/kg, C_s evaluated from the experimental results was about half of the analytical estimated value, with a maximum value of $C_s = 700\,\mathrm{MJ/m^3}$.

Inadequate wetting is also discussed in the literature. For example, Keßling et al. [8] studied an internally cooled absorber for isothermal conditions. They explained the deviation between their model and measured data with incomplete wetting of the absorber plates and reported a wetting fraction of about 30%. The wetting fraction was defined as the ratio between the visually detected wetted area and the dry area during absorption measurements.

The mean desiccant mass flow rate of $\dot{m}_{sol} = 38$ kg/h in the present intermitted flow experiment is about twice as high as the mass flow rate used in the experiments performed by Keßling et al. [8]. In turn, a higher wetting factor was reached in the measurements presented above compared to the values by Keßling et al. since the wetting of the textile is in generally improved by increasing the solution flow rate.

6 Conclusions

A solar-assisted liquid desiccant system was designed and constructed at the Hessian State Domain Frankenhausen, Germany. A novel plate absorber (dehumidifier) was designed with textiles attached to the walls to reduce desiccant flow rates and enhance wetting of the exchange plates. Wetting of the absorber plates was improved compared to earlier systems investigated and reported in the literature. The absorber was operated in the demonstration plant on different days and in different seasons of the year.

The moisture removal rate and the absorber effectiveness were used as the performance indices of the absorber. Furthermore, the volumetric energy storage capacity was evaluated as a function of the desiccant flow rate. For summer outdoor conditions, moisture removal rates of up to 4.7 kg/h were reached associated with a temperature increase of the supply air of up to 8.5 K.

In additional investigations, the desiccant solution was pumped in the absorber in an intermittent mode in order to reach higher energy storage capacities and to improve the wetting of the contact surface. In the performed experiment, a mass fraction spread of about 13% points and an energy storage capacity of about $900\,\mathrm{MJ/m^3}$ was reached.

A numerical model was used to compare the experimental results with theoretical values. The modeling results show the same tendencies as the experimental results; however, the absolute values for the modeled effectiveness and moisture removal rate are clearly higher due to the idealizations taken in the model. Therewith, the comparison of measured and numerical values shows the optimization potential for the absorber construction and operation.

The present work shows that solar-assisted liquid desiccant systems are applicable for a gentle drying of agricultural products.

Acknowledgment

The financial support of the German Federal Ministry for Education and Research (BMBF) within the research project "OpenSorp" is gratefully acknowledged. Moreover, the authors thank the Hessian State Domain Frankenhausen for their support of the research.

Funding Data

- Bundesministerium fuer Bildung und Forschung (AZ 03SF 0444- OpenSorp, and FK 01 LR0809B- KlimZug).

Nomenclature

A = area, $\mathrm{m^2}$
C_s = energy storage capacity, $\mathrm{MJm^{-3}}$
C = heat capacity rate, $\mathrm{Js^{-1}K^{-1}}$
D = diffusion coefficient, $\mathrm{m^2s^{-1}}$
g = gravitational acceleration, $\mathrm{m^2s^{-2}}$
h = specific enthalpy, $\mathrm{Jkg^{-1}}$
κ_m = mass balance factor
M = mean absolute deviation
M = molar mass, $\mathrm{kgmol^{-1}}$
$\dot{m}$ = mass flow rate, $\mathrm{kgh^{-1}}$
n = amount of substance, mol

Nu = Nusselt number
p = pressure, Pa
$\dot{Q}$ = rate of heat flow, Js^{-1}
r_m = air to solution mass flow ratio
Re = Reynolds number
$\dot{V}$ = volume flow rate, m^3h^{-1}
v_x, v_y, v_z = velocity components in the respective spatial direction, ms^{-1}
x = distance in direction of the flow (solution), m
X = mass of water per mass of LiCl salt, $kg_{H2O}kg_{LiCl}^{-1}$
y = distance in direction of the flow (air), m
z = transverse direction to the streams, distance from the absorber plate, m
Δ = difference
ε = effectiveness
γ = viscosity
ξ = mass fraction of the desiccant, $kg_{LiCl}kg_{sol}^{-1}$
λ = thermal conductivity, $Wm^{-1}k^{-1}$
ρ = density, kgm^{-3}
ϑ = temperature, °C
φ = relative humidity
ω = humidity ratio, $g_w kg_{dry\,air}^{-1}$

Subscripts

a = air
cond = conduction
conv = convection
e = equilibrium
in = inlet conditions
o = outlet conditions
s = saturated
sim = simulation
sol = solution
v = water vapor
w = liquid water

Abbreviations

AS = air side
da = dry air
dil = diluted
SS = solution side

References

[1] Misha, S., Mat, S., Ruslan, M. H., Salleh, E., and Sopian, K., 2016, "Performance of a Solar Assisted Desiccant Dryer for Oil Palm Fronds Drying," Sol. Energy, **132**(216), pp. 415–429.
[2] Misha, S., Mat, S., Ruslan, M. H., and Sopian, K., 2012, "Review of Solid/Liquid Desiccant in the Drying Applications and Its Regeneration Methods," Renewable Sustainable Energy Rev., **16**(7), pp. 4686–4707.
[3] Karam, M., Petit, J., Zimmer, D., Djantou, E., and Scher, J., 2016, "Effects of Drying and Grinding in Production of Fruit and Vegetable Powders: A Review," J. Food Eng., **188**, pp. 32–49.
[4] Badgujar, V., 2012, "An Experimental Investigation of Solar Dryer With Regenerative Desiccant Material for Multicrops," Int. J. Eng. Res. Appl., **2**(3), pp. 3144–3149.
[5] Misha, S., Mat, S., Ruslan, M. H., Salleh, E., and Sopian, K., 2015, "Performance of a Solar Assisted Desiccant Dryer for Kenaf Core Fiber Drying Under Low Solar Radiation," Sol. Energy, **112**, pp. 194–204.
[6] Madhiyanon, T., Adirekrut, S., Sathitruangsak, P., and Soponronnarit, S., 2007, "Integration of a Rotary Desiccant Wheel Into a Hot-Air Drying System: Drying Performance and Product Quality Studies," Chem. Eng. Process., **46**(4), pp. 282–290.
[7] Oberg, V., and Goswami, D., 1998, "Experimental Study of the Heat and Mass Transfer in a Packed Bed Liquid Desiccant Air Dehumidifier," ASME J. Sol. Energy Eng., **120**, pp. 289–97.
[8] Keßling, W., Lävemann, E., and Kapfhammer, C., 1998, "Energy Storage for Desiccant Cooling Systems Component Development," Sol. Energy, **64**(4–6), pp. 209–221.
[9] Ertas, A., Gandhidasan, P., Kiris, I., and Anderson, E., 1994, "Experimental Study on the Performance of a Regeneration Tower for Various Climatic Conditions," Sol. Energy, **53**(1), pp. 125–130.
[10] Elsarrag, E., 2006, "Performance Study on a Structured Packed Liquid Desiccant Regenerator," Sol. Energy, **80**(12), pp. 1624–1631.
[11] Gandhidasan, P., 2005, "Quick Performance Prediction of Liquid Desiccant Regeneration in a Packed Bed," Sol. Energy, **79**(1), pp. 47–55.
[12] Gommed, K., and Grossman, G., 2007, "Experimental Investigation of a Liquid Desiccant System for Solar Cooling and Dehumidification," Sol. Energy, **81**(1), pp. 131–138.
[13] Gommed, K., and Grossman, G., 2004, "A Liquid Desiccant System for Solar Cooling and Dehumidification," ASME J. Sol. Energy Eng., **126**(3), pp. 879–885.
[14] Gommed, K., Grossman, G., and Ziegler, F., 2004, "Experimental Investigation of a LiCl-Water Open Absorption System for Cooling and Dehumidification," ASME J. Sol. Energy Eng., **126**(2), pp. 710–715.
[15] Lowenstein, A., 2008, "Review of Liquid Desiccant Technology for HVAC Applications," HVACR Res., **14**(6), pp. 819–839.
[16] Lowenstein, A., Slayzak, S., Kozubal, E., Feldman, S., and Tandler, J., 2006, "A Zero-Carryover Liquid Desiccant Air Conditioner for Solar Applications," ASME Paper No. ISEC2006-99079.
[17] Lowenstein, A., Slayzak, S., Ryan, J., and Pesaran, A., 1998, "Advanced Commercial Liquid Desiccant Technology Development Study," National Renewable Energy Laboratory, Golden, CO.
[18] Lävemann, E., Keßling, W., Röhle, B., and Kink, C., 1996, "Klimatisierung über Sorption, Endbericht zur Phase I des Forschungsvorhabens," B des BMFT, Fraunhofer Instituts für Solare Energiesysteme, Freiburg und Ludwig-Maximilians-Universität München, Sektion Physik, LS Prof. Sitzmann, München, Germany, Report Nr. 032 9151.
[19] Lävemann, E., Keßling, W., and Peltzer, M., 1996, "Solarunterstützte Klimatisierung über Sorption, Endbericht zur Phase II des Forschungsvorhabens," F des BMBF, Bayerisches Zentrum für Angewandte Energieforschung e.V., München, Germany, Nr. 032 9151.
[20] Hublitz, A., 2008, "Efficient Energy Storage in Liquid Desiccant Cooling Systems," Ph.D. thesis, Technische Universität München, München, Germany.
[21] Abdel-Salam, A., McNevin, C., Crofoot, L., Harrison, S., and Simonson, C., 2016, "A Field Study of a Low-Flow Internally Cooled/Heated Liquid Desiccant Air Conditioning System: Quasi-Steady and Transient Performance," ASME J. Sol. Energy Eng., **138**(3), p. 031009.
[22] Jaradat, M., 2016, "Construction and Analysis of Heat-and Mass Exchangers for Liquid Desiccant Systems," Ph.D. thesis, University of Kassel, Kassel, Germany.
[23] Román, F., and Hensel, O., 2014, "Numerical Simulations and Experimental Measurements on the Distribution of Air and Drying of round Hay Bales," Biosyst. Eng., **122**, pp. 1–15.
[24] ASHRAE, 1997, *Handbook – Fundamentals*, American Society of Heating, Refrigerating and Air-Conditioning Engineers, Atlanta, GA.
[25] Conde, M. R., 2004, "Properties of Aqueous Solutions of Lithium and Calcium Chlorides: Formulations for Use in Air Conditioning Equipment Design," Int. J. Therm. Sci., **43**(4), pp. 367–382.
[26] Mützel, M., 2009, "Modellierung Eines Im Kreuzstrom Betriebenen Sorptionsreaktor Für Sorptionsgestützte Klimatisierungsanlagen," Masterarbeit, Maschinenbau, Universität Kassel, Institut für thermische Energietechnik, Kassel, Germany.
[27] Mesquita, L., Harrison, S. J., and Thomey, D., 2006, "Modeling of Heat and Mass Transfer in Parallel Plate Liquid-Desiccant Dehumidifiers," Sol. Energy, **80**(11), pp. 1475–1482.
[28] Liu, X. H., Zhang, Y., Qu, K. Y., and Jiang, Y., 2006, "Experimental Study on Mass Transfer Performances of Cross Flow Dehumidifier Using Liquid Desiccant," Energy Convers. Manage., **47**(15–16), pp. 2682–2692.
[29] Mesquita, L., 2007, "Analysis of a Flat-Plate Liquid-Desiccant Dehumidifier and Regenerator," Ph.D. thesis, Queen's University, Kingston, ON, Canada.